Ciesielski, P. F., Kristoffersen, Y., et al., 1991
Proceedings of the Ocean Drilling Program, Scientific Results, Vol. 114

36. PHYSICAL PROPERTIES OF SEDIMENTS BENEATH POLAR FRONT UPWELLING REGIONS IN THE SUBANTARCTIC SOUTH ATLANTIC (HOLE 704A)[1]

Jürgen Mienert[2] and David Nobes[3]

ABSTRACT

The physical properties of sediments beneath an upwelling area in the southern part of the Atlantic Ocean (ODP Hole 704A) were investigated. Highly significant correlations characterize the relationship of carbonate content to bulk density ($R = 0.85$), carbonate content to porosity ($R = 0.84$), and carbonate content to impedance ($R = 0.84$). No relationship exists between carbonate content and compressional-wave velocity ($R = 0.24$), indicating that amplitude variations in impedance are primarily controlled by variations in bulk density, which, in turn, are controlled by climatically driven biogenic opal and carbonate deposition. In general, maxima in impedance correspond to maxima in carbonate content (minima in opal content). The impedance record exhibits its most drastic change at about 2.4 Ma, marking dramatic increases in the average content of biogenic opal and the beginning of large-amplitude fluctuations. Between 0.7 and 0.4 Ma carbonate content, bulk density, and grain density decrease while opal content drastically increases. Similar changes have been observed in sediments beneath an upwelling cell off northwest Africa, indicating an oceanwide enhancement in upwelling or in the calcite corrosiveness of bottom water that appears to be isochronous.

INTRODUCTION

The aim of this study is to investigate the characteristics of the physical properties of sediments deposited beneath an oceanic upwelling province at the Polar Front in the southern part of the Atlantic Ocean (Fig. 1). Sediment physical properties depend to a large extent on grain size and proportion of the sediment components clay, quartz, biogenic carbonate, and silica, which, in turn, are controlled by environmental factors (e.g., Mayer, 1979; Hamilton et al., 1982; Nobes et al., this volume). In particular, dissolution of biogenic sediments, dilution by nonbiogenic material, changes in biogenic productivity, and current winnowing control their distribution (e.g., Berger and Mayer, 1978; Mienert et al., 1988). How past changes in the productivity of surface waters affected the distribution of sediment components and thus the physical properties is the focus of our investigation. In this paper we concentrate on the distribution of biogenic silica, carbonate content, and grain size to determine the changes in pelagic sediments that may affect the physical and acoustical properties of sediments, in particular, acoustic impedance.

For this purpose we investigated Ocean Drilling Program (ODP) Hole 704A, drilled on the Meteor Rise (46°52.75′S, 07°25.25′E) at a water depth of 2532 m. The site location is above the carbonate compensation depth (CCD) and in the range of the Polar Front, an oceanic boundary where the upwelling of cold, nutrient-rich water causes an increase in oceanic productivity and thus in biogenic silica, which accumulates on the seafloor. The boundary divides the sedimentological environment of the southern part of the Atlantic Ocean between calcareous ooze to the north and dominantly biosiliceous ooze to the south. Distinct changes in the development and movement of the Polar Front should be documented in both the sedimentological record and the physical-property record.

METHODS

The sediment fraction <63 μm was separated from the fraction >63 μm by sieving. The subfractions <63 μm were examined using a Sedigraph 5000D (Stein, 1985; Micromeritics, 1978). The instrument measures the size distribution of particles dispersed in a liquid by assuming velocities of sinking particles in a viscose fluid (Stokes' law), as shown schematically in Figure 2. Carbonate determinations were made aboard ship with a Coulometrics Carbon Analyzer, which measures the carbon dioxide released upon acidification of a sample. The relative precision of the data is ±2%.

Physical and acoustical properties of sediments were also determined aboard ship immediately after the sediment cores reached room temperature (22°C). Wet-bulk density, dry-bulk density, water content, grain density, and porosity were determined by gravimetric techniques (Hamilton, 1971). Samples of 5 to 10 cm^3 were taken in precalibrated aluminum beakers from undisturbed sediments. Wet and dry weights were determined using a Scitech Electronic Balance to a precision of ±0.01 g. The measurements were reproducible to ±0.04 g. Sample volumes were determined for both wet and dry samples using the Penta Pycnometer, with a precision of 10^{-4} cm^3. The wet samples were oven dried at 100°C for 24 hr. The physical properties were then computed using weight and volume as outlined by Hamilton (1971).

Compressional-wave velocity measurements were conducted on split cores within the liner (Boyce, 1976). The calibration of velocities agreed within estimated errors, that is, ±50 m/s after removal of time delays caused by the liner and the cable. Measurements were generally reproducible to within ±20 m/s.

Drilling disturbance was encountered at Hole 704A, particularly between 20 and 40 m below seafloor (mbsf). Samples were taken only from intervals that we visually identified as undisturbed. The possibility exists, however, that slightly disturbed areas were not recognized because they are difficult, if not impossible, to detect.

[1] Ciesielski, P. F., Kristoffersen, Y., et al., 1991. *Proc. ODP, Sci. Results*, 114: College Station, TX (Ocean Drilling Program).
[2] GEOMAR, Forschungszentrum der Christian-Albrechts-Universität zu Kiel, D-2300 Kiel, FRG.
[3] University of Waterloo, Department of Earth Sciences, Waterloo, Ontario, Canada N2L 3G1.

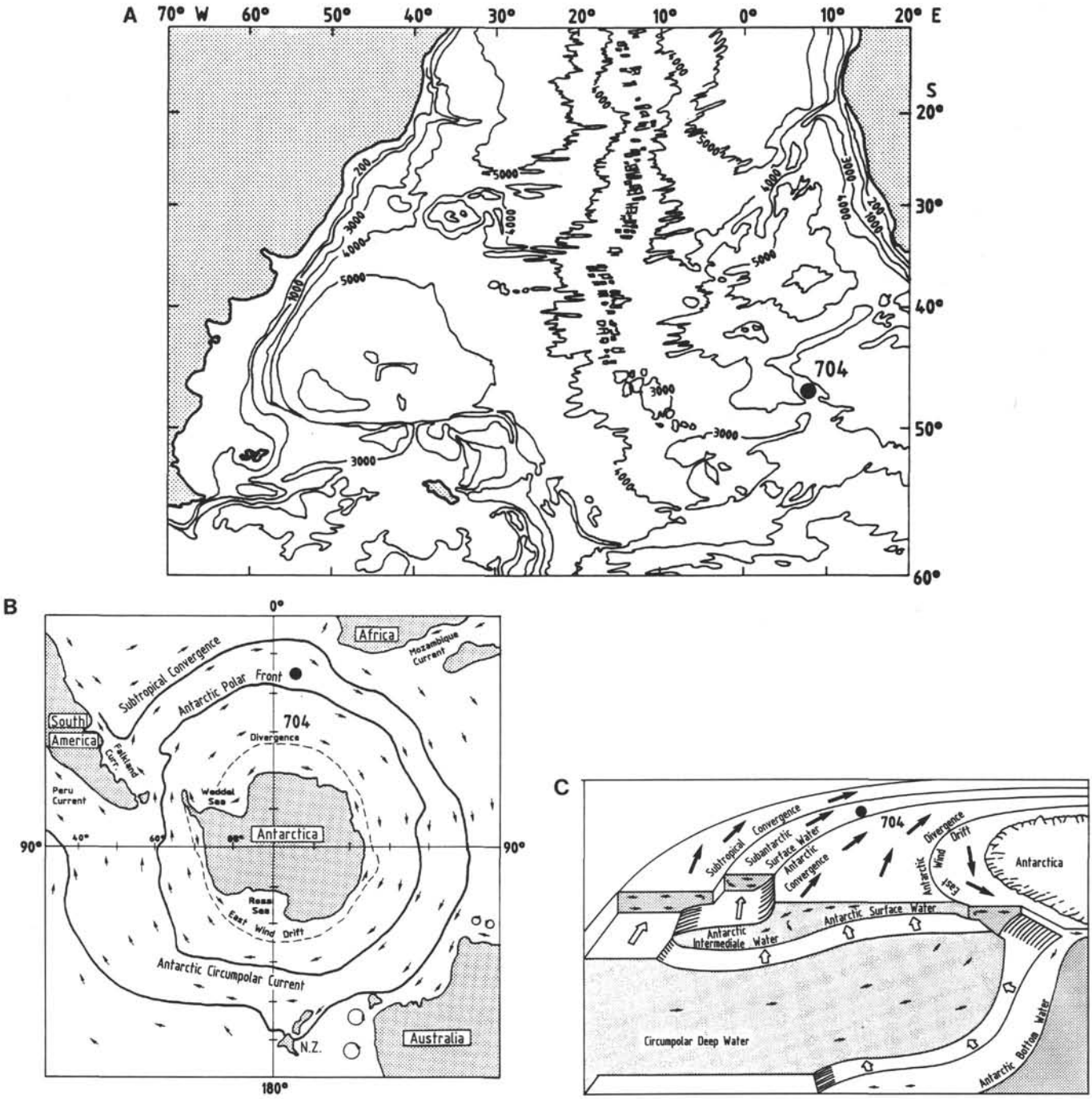

Figure 1. **A.** Location map of ODP Site 704 in the southern part of the Atlantic Ocean. **B.** Present-day Southern Ocean circulation (from Pickard and Emery, 1982). **C.** Schematic cross section of major surface and subsurface water masses of the Southern Ocean (from Gordon, 1971) (Antarctic Convergence is equivalent to the Polar Front).

Chronostratigraphic datum levels (Table 1) are used to plot the age vs. depth curve (Fig. 3). The depths of the magnetic reversals are from Hailwood and Clement (this volume), and those for diatom levels are from Fenner (this volume). By assuming constant sedimentation rates between the datum levels, a linear interpolation allows us to transfer the physical-properties depth records into age records. Because the apparent age of the top of Hole 704A is at least 0.195 Ma (Ciesielski, Kristoffersen, et al., 1988) some age uncertainties exist in the uppermost part of the hole. There is an indication that the topmost portion of the hole (latest Pleistocene) is missing (Froelich et al., this volume).

RESULTS AND DISCUSSION

Carbonate content and grain density (Fig. 4) show similar characteristic trends in which low concentrations in carbonate correspond to low values in grain density. This is due to the fact that the principal noncarbonate dilutant is biogenic silica, which has a low grain density, ranging on average from 1.7 to 2.2 g/cm^3 (e.g., Hurd and Theyer, 1977). The

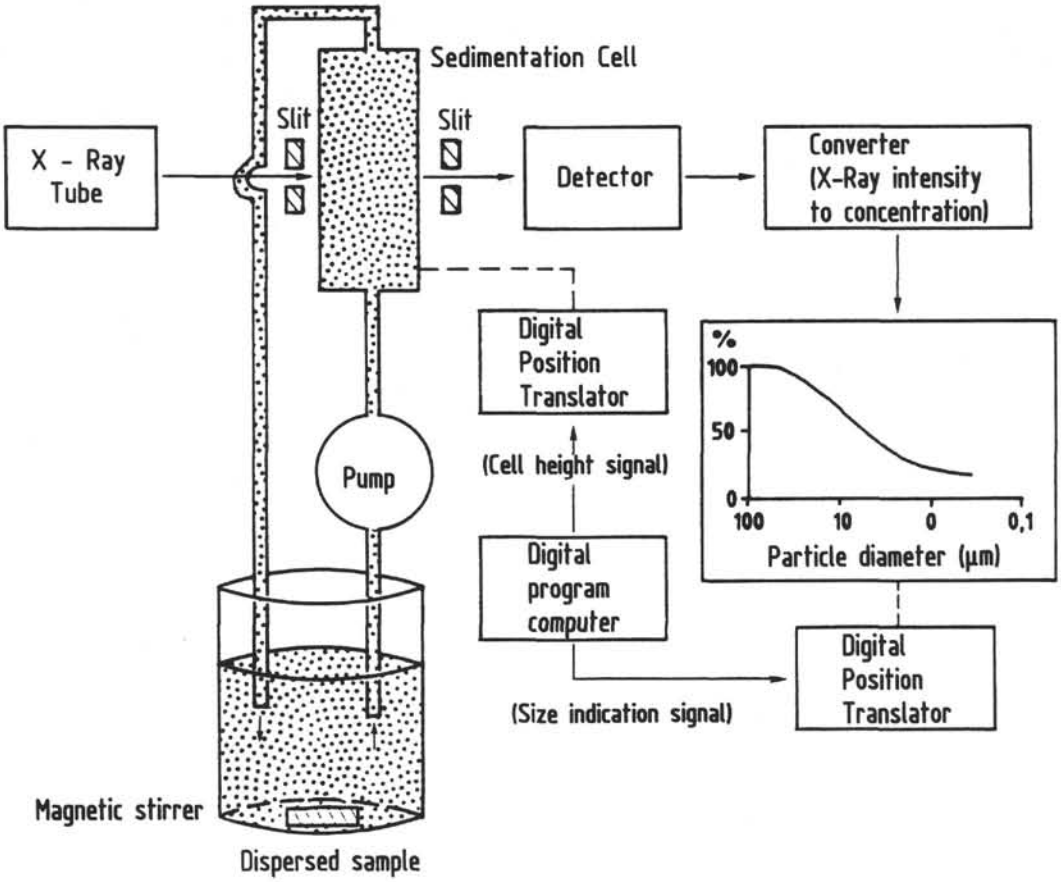

Figure 2. Diagram of the SediGraph 5000D. The attenuation of an X-ray beam through suspended particles is electronically transformed into concentration values.

Table 1. Chronostratigraphic datum levels, Hole 704A.

Depth (mbsf)	Age (Ma)	Interval in Hole 704A	Microfossil and paleomagnetic datums[a]
3.88	0.195	1H-2, 100 cm, to 1H-3, 76 cm	LAD *Hemidiscus karstenii*
15.15	0.62	2H-5, 120 cm, to 2H-5, 120 cm	LAD *Actinocyclus ingens*
33.10	0.73	3H-5, 99 cm, to 5H-7, 16 cm	Brunhes/Matuyama boundary
93.70	1.66	11H-1, 16 cm, to 11H-2, 34 cm	Top Olduvai subchron
100.73	1.89	11H-6, 35 cm, to 11H-6, 80 cm	LAD *Coscinodiscus kolbei*
144.01	2.20	16H-4, 60 cm, to 16H-2, 62 cm	LAD *Coscinodiscus vulnificus*
168.45	2.47	18X-6, 145 cm, to 19X-1, 5 cm	Matuyama/Gauss boundary
169.14	2.64	18X-6, 78 cm, to 19X-2, 60 cm	LAD *Nitzschia weaveri*
176.15	2.92	19X-5, 135 cm, to 19X-6, 5 cm	Top Kaena Subchron
178.20	2.99	19X-7, 5 cm, to 19X-7, 15 cm	Base Kaena Subchron
179.10	3.08	20X-1, 85 cm, to 20X-1, 95 cm	Top Mammoth Subchron
181.55	3.18	20X-3, 25 cm, to 20X-3, 45 cm	Base Mammoth Subchron
186.60	3.40	20X-6, 85 cm, to 20X-6, 95 cm	Gauss/Gilbert boundary
198.45	3.88	22X-1, 115 cm, to 22X-1, 135 cm	Top Cochiti Subchron
202.15	3.97	22X-4, 15 cm, to 22X-4, 75 cm	Base Cochiti Subchron
204.20	4.10	22X-5, 95 cm, to 22X-5, 104 cm	Top Nunivak Subchron
210.45	4.24	23X-3, 65 cm, to 23X-3, 75 cm	Base Nunivak Subchron
212.00	4.40	23X-4, 75 cm, to 23X-4, 85 cm	Top Sidufjall Subchron
213.30	4.47	23X-5, 55 cm, to 23X-5, 65 cm	Base Sidufjall Subchron
217.25	4.57	24X-1, 55 cm, to 24X-2, 5 cm	Top Thvera Subchron
219.45	4.77	24X-3, 15 cm, to 24X-3, 35 cm	Base Thvera Subchron

Note: Depths for magnetic reversals from Hailwood and Clement (this volume) and for diatom levels from Fenner (this volume).
[a] FAD = first-appearance datum; LAD = last-appearance datum.

records show some resemblance to those of ODP Site 658, located beneath an upwelling cell off northwest Africa, where low carbonate concentrations (<50%) and low grain-density values (<2.6 g/cm^3) also indicate a dilution by biogenous silica. The low grain-density values occur during the time intervals from 2.4 to 1.8 Ma and from 0.7 to 0.4 Ma (Mienert and Schultheiss, 1989).

At Hole 704A, the most drastic changes in carbonate content and sediment physical properties occur between 100 and 80 mbsf and near 20 mbsf (Fig. 4). From 220 to 100 mbsf carbonate concentrations are relatively high (>50%). The bulk density increase and water content and porosity decreases with depth are associated with a normally consolidating sediment. As a result, dry-bulk density has an average gradient of 0.23 g/cm^3/100 m and porosity has an average gradient of 8.12%/100 m. An abrupt decrease in carbonate content (from 70% to 15%) at 100 mbsf corresponds to a distinct decrease in grain density (from 2.7 to 2.3 g/cm^3) and wet-bulk density (from 1.6 to 1.3 g/cm^3) and to a high in water content (from 50% to 70%) and porosity (from 70% to 85%) (Fig. 4). These changes mark the lower boundary of an interval that extends from 100 to 40 mbsf. It is characterized by generally low values in carbonate content (<50%) and only slightly variable values in bulk density, water content, and porosity. This pattern is due to the presence of appreciable amounts of biogenic silica that may cause a sediment framework where the mechanical interlocking of open-structured microfossils hinders consolidation processes. Mayer (1982) reported a similar behavior of sediment physical properties beneath the equatorial upwelling zone in the Pacific Ocean, where biogenous silica concentrations maintain high porosities and water contents and very low saturated bulk densities and shear strengths for more than 200 m. He pointed out that the most significant factor controlling the physical properties of unconsolidated sediments is the presence or absence of biogenic silica.

Percentages of sand grain sizes >63 µm (Fig. 4) show large-amplitude fluctuations between 0% and 40% throughout

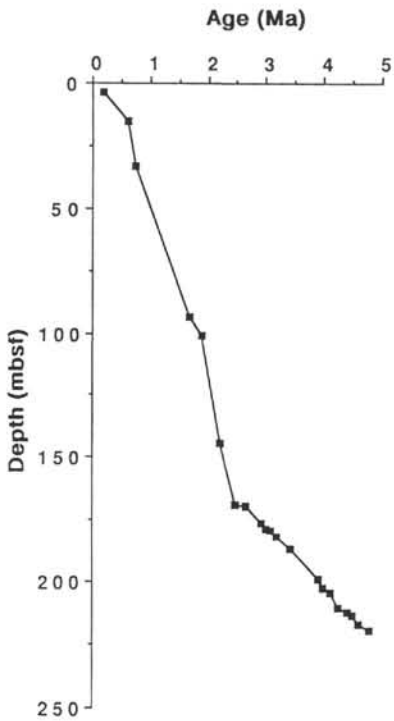

Figure 3. Age vs. depth plot derived from chronostratigraphic datum levels, Hole 704A (Table 1).

the sediment column. There is some consistency between high percentages of sand and high percentages of carbonate. Similar trends, for instance, have been observed in Quaternary sediments of the equatorial Atlantic where planktonic foraminifers are the dominant components in the sediment fraction >63 μm (e.g., Mienert et al., 1988). Complex processes of productivity and dissolution of carbonate there control the percentage of sand grain sizes, which, in turn, controls the variability of compressional-wave velocities in a distinctive manner. High velocities occur during interglacial times with a high percentage of carbonate, and the prevailing sand grain size is the result of a diminished carbonate dissolution. Low velocities correspond to glacial times in which primarily low percentages of carbonate and sand grain sizes persist.

That no such correlations were observed between carbonate content and compressional-wave velocity at Hole 704A (R = 0.24) (Fig. 5B) is possibly due to the fact that the sediment rigidity is dominantly controlled by a framework of biogenic silica rather than by the grain sizes of the carbonate material. The relationship of bulk density (wet and dry) to carbonate content (Fig. 5A) shows a systematic trend and a significant correlation (R = 0.86). A similar relationship was observed in upper Quaternary sediments of the eastern equatorial Atlantic (Curry and Lohmann, 1986), an area of oceanic upwelling where appreciable amounts of biogenic silica exist (Mienert, 1986). The relationship between bulk density and carbonate content also parallels the relationship of eastern equatorial Pacific samples (Kominz et al., 1977; Mayer, 1979). These high-productivity regions of the world oceans appear to be characterized by a unique and consistent pattern of positive carbonate content to bulk density relationships. Most importantly, they may significantly influence the acoustic stratigraphy of sediments beneath upwelling areas, as seen in the correlation between carbonate content and impedance (Fig. 5C). Acoustic events there should be controlled by drastic changes in wet-bulk density and thus carbonate content, which, in turn, are mainly controlled by the concentration of biogenic silica.

In the subfractions <63 μm (Fig. 6 and Table 2) a progressive increase occurs from silt- toward clay-size material. Very low average values exist in the 63- to 50-μm fraction and very high average values are in the <2-μm fraction. Maxima and minima of the <2-μm fraction do not correlate with the other subfractions. Generally, the peaks in the percent grain-size fractions can be correlated neither to each other nor to the most drastic changes in the physical properties, which occur at 100 and 40 mbsf and at 20 and 10 mbsf (Fig. 4). These changes in physical properties correspond more to changes in the >63-μm grain-size fraction (Fig. 4) than to changes in the subfractions (Fig. 6).

Carbonate content, grain density, bulk density (wet and dry), water content, and porosity for the last 4.8 Ma are displayed as a function of age in Figure 7. From 4.8 to 1.9 Ma average carbonate concentrations are relatively high (>50%) and low-amplitude variations prevail.

Beginning at about 2.4 Ma the amplitudes in carbonate content become significant. They show distinct minima between 1.9 Ma and the present (Fig. 7). The most prominent minima occur between 1.9 and 1.4 Ma (15%) and between 0.7 and 0.4 Ma (35%). Each of these is present as a minimum in the grain-density record as well, indicating that they are due to increased concentrations of biogenic silica. This, in turn, may be caused by enhanced biological production of silica or by dissolution of carbonate, or a combination of both. We also envision a movement of the Polar Front to the north, which expands the biosiliceous province across the site location. However, Froelich et al. (this volume) have shown that most of the minima in the concentration of carbonate correspond to maxima in the record of the percentage of other components, indicating that they reflect horizons of carbonate dissolution. Between 0.8 and 0.7 Ma is a prominent maximum in carbonate content. Its lack of appreciable amounts of biogenic silica probably suggests a more southward position of the Polar Front.

Beginning at 1.9 Ma, the physical-properties records of bulk density, water content, and porosity show prominent changes that correspond to changes in carbonate content. At 1.9 Ma, dry-bulk density decreases (from 0.75 to 0.5 g/cm^3) with a concurrent decrease in carbonate (from 70% to 15%). A 55% difference in percent carbonate causes a difference in bulk density of 0.25 g/cm^3. From 1.9 to 0.75 Ma bulk density remains low (0.5 g/cm^3), and it increases (from 0.5 to 0.75 g/cm^3) between 0.75 and 0.4 Ma. The water content and porosity records show similar changes but with opposite trends: they decrease with an increase in carbonate content.

The effect of carbonate and opal concentration (Froelich et al., this volume) on acoustic impedance is seen in Figure 8. In order to establish a baseline for the acoustic stratigraphy of Neogene upwelling areas of the world ocean, it is necessary to determine the time intervals and the magnitude at which the most drastic changes in acoustic impedance occur and how they correspond to paleoceanographic events. A detailed acoustic impedance profile was not constructed because (1) samples with both compressional-wave velocity and wet-bulk density measurements exist only for intervals >3 m and (2) velocity and density logging runs are lacking in the upper 150 mbsf of the borehole, where they would be extremely useful for detailed calculations of impedance.

Generally, the impedance peaks correlate to intervals with low percentages of opal. An exception occurs at 13 mbsf, where an impedance peak corresponds to a high opal content. The calculated impedance record (wet-bulk density × compressional-wave velocity) shows a characteristic min-

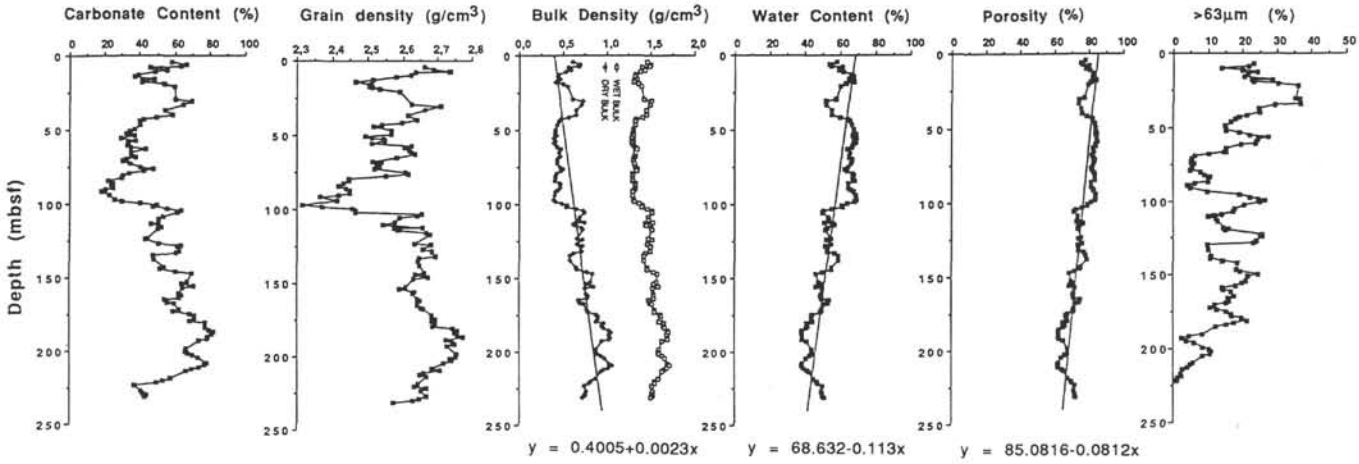

Figure 4. Carbonate content, grain density, bulk density, water content, porosity, and grain size vs. depth. The lines through the data are the best first-order fits, which show the change in physical properties related to a consolidating sediment.

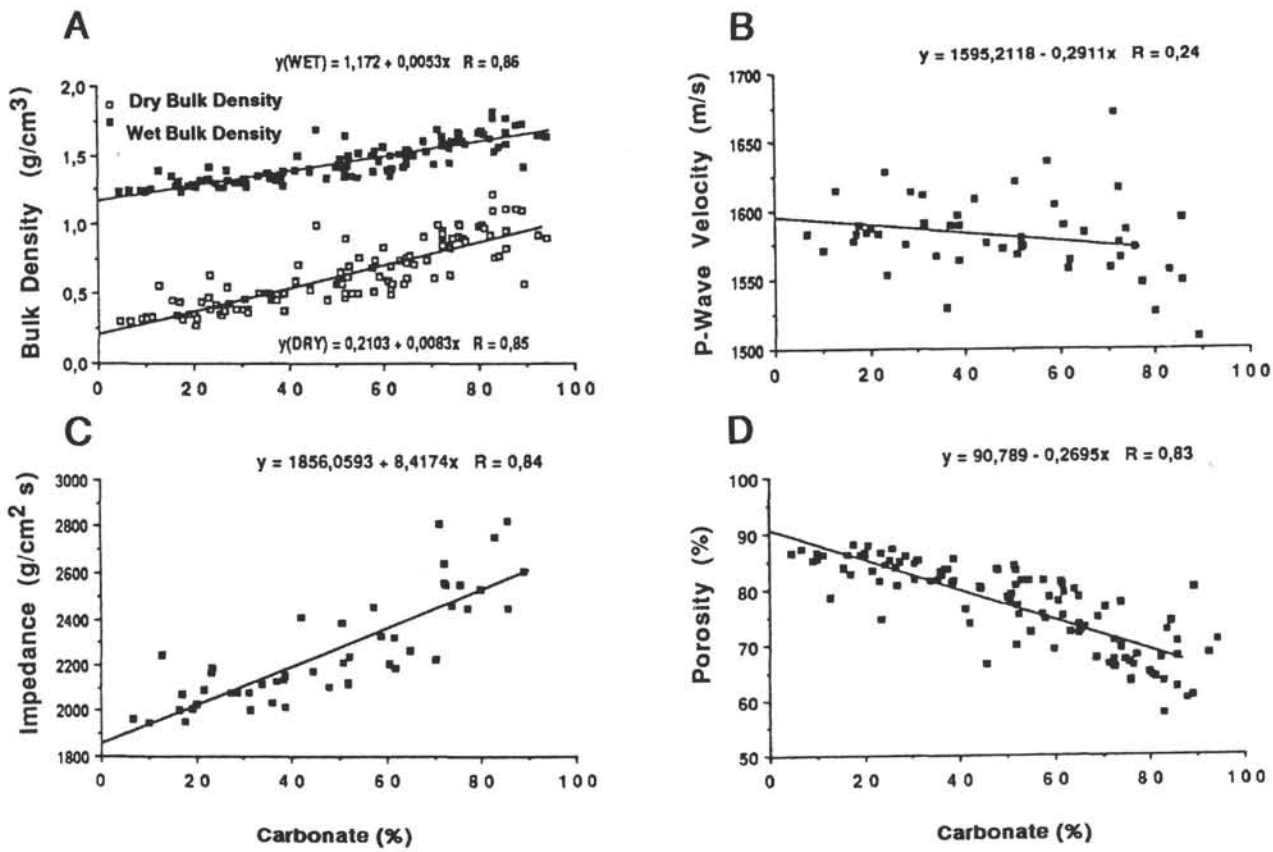

Figure 5. Physical-properties relationships. **A.** Dry-bulk and wet-bulk density to carbonate content. **B.** Compressional-wave velocity to carbonate content. **C.** Impedance to carbonate content. **D.** Porosity to carbonate content.

imum between 150 and 125 mbsf that corresponds to a drastic increase in opal content and a concurrent decrease in carbonate content (Fig. 8). The other components show no distinct change in comparison with the high-amplitude variations in opal and carbonate content. However, a major phase of ice rafting is documented at this particular depth interval starting at about 2.45 Ma (Allen and Warnke, this volume).

Below 150 mbsf the impedance record shows large fluctuations ranging from 2.25×10^5 to 3.25×10^5 g/cm²s. They are located directly beneath a sedimentological break that is a transition from low (<15%) to high (>15%) average opal concentrations. We therefore anticipate that the relative changes in opal content contribute to the changes in impedance. Most importantly, the percentage of other sediment components has no or only a minor influence on the acoustic impedance. Changes in acoustic impedance appear to be entirely controlled by changes in carbonate content ($R = 0.85$; Fig. 5C). However, we must await further results before we can elaborate more fully on the relationship between the depositional environment beneath upwelling regions and the acoustic record.

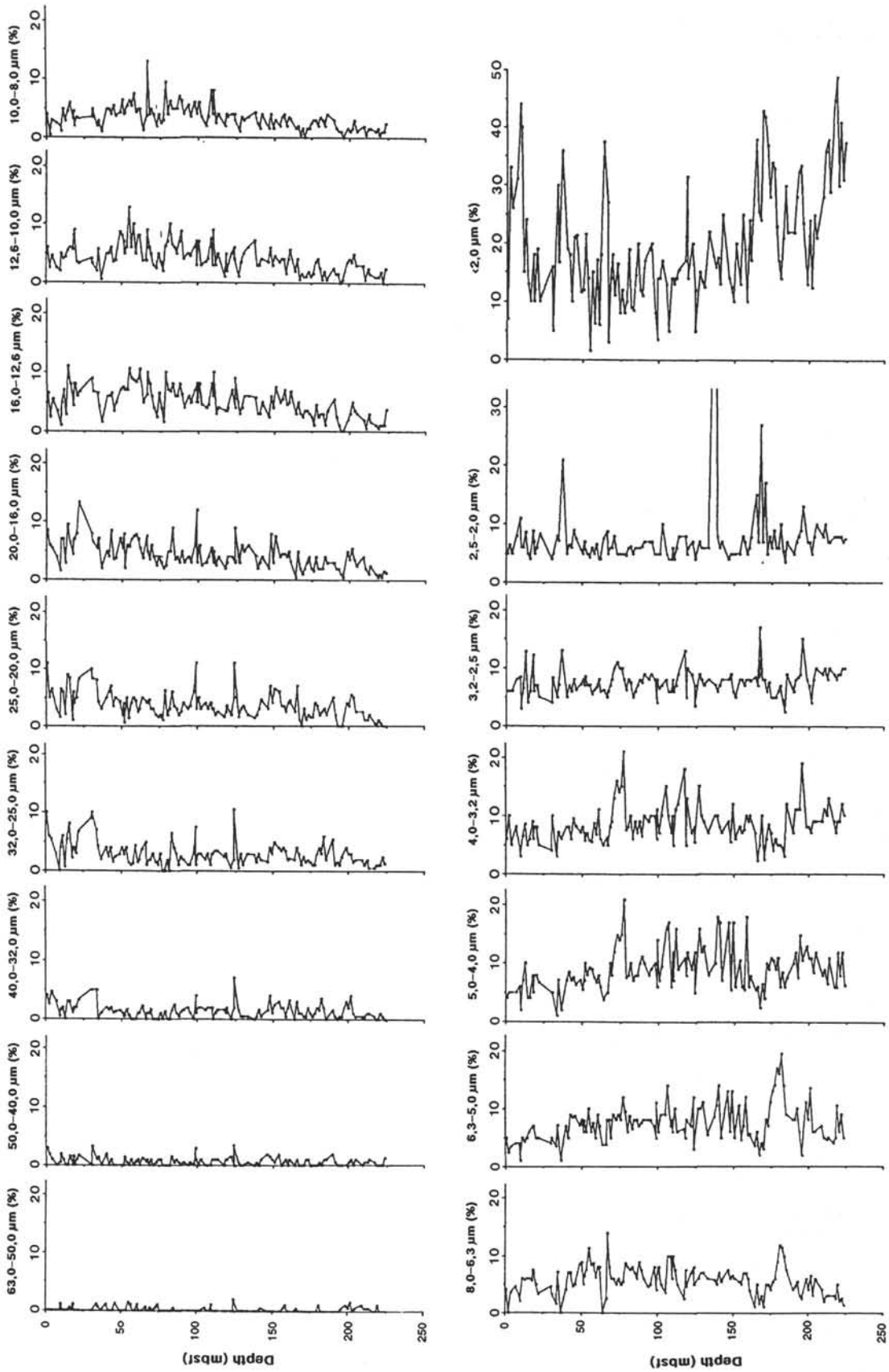

Figure 6. Subfractions of grain sizes <63 µm vs. depth (Table 2).

We converted the impedance peaks from depth to age by using the age vs. depth plot (Fig. 3). Thirteen peaks were determined and time calibrated. It is important to note that the record may be subject to revisions if the sampling interval changes. However, the peaks correlate with the following (approximate) changes in the sedimentological record (Table 3).

In terms of paleoceanographic events the most drastic changes in the impedance record (Fig. 8) occur between 2.4 and 1.9 Ma. They possibly correspond to a major phase of ice rafting (Allen and Warnke, this volume) and an enhancement of upwelling documented in an increase in biogenic silica concentration. From 0.7 to 0.4 Ma is a distinct minimum in carbonate content and bulk density that has been observed beneath the eastern equatorial Atlantic upwelling regions (Site 658; Mienert and Schultheiss, 1989), suggesting a synchronous paleoceanographic event.

CONCLUSIONS

Carbonate content to bulk density relationships ($R = 0.85$) are positive beneath regions of high biological production in the Atlantic and Pacific oceans (Mayer, 1979) where the principal noncarbonate dilutant is biogenic silica.

Major changes in the concentration of both carbonate and opal correlate to changes in acoustic impedance ($R = 0.84$). Our results from the southern part of the Atlantic Ocean are similar to those from Pacific (e.g., Mayer, 1979) and equatorial Atlantic upwelling regions (e.g., Mienert, 1986). Thus the paleoceanographic history of climatically driven upwelling regions can be preserved in acoustic records. They are important tools for deciphering the lateral extent and the history of biogenic sedimentation.

A distinct low in both carbonate content and grain density between 0.7 and 0.4 Ma occurring beneath upwelling regions of the eastern equatorial Atlantic (Hole 658A) and the southern part of the Atlantic Ocean (Hole 704A) may correspond to an oceanwide increase in carbonate dissolution and/or upwelling intensity.

ACKNOWLEDGMENTS

We are thankful to Don Sims and Kevin Rogers, who helped run the shipboard physical-property measurements. Technical support for the grain-size analyses was provided by Uwe Grützmacher and Andreas Wittmark. The authors are grateful to L. A. Mayer and T. C. Moore for reviewing the manuscript. The research was sponsored by JOI grant TAMRF-20136.

REFERENCES

Berger, W., and Mayer, L. A., 1978. Deep-sea carbonates: acoustic reflectors and lysocline fluctuations. *Geology*, 6:11–15.

Boyce, R. E., 1976. Definitions and laboratory techniques of compressional sound velocity parameters and wet-water content, wet-bulk density, and porosity parameters by gravimetric and gamma ray attenuation techniques. *In* Schlanger, S. O., Jackson, E. D., et al., *Init. Repts. DSDP*, 33: Washington (U.S. Govt. Printing Office), 931–958.

Ciesielski, P. F., Kristoffersen, Y., et al., 1988. *Proc. ODP, Init. Repts.*, 114: College Station, TX (Ocean Drilling Program).

Curry, W. B., and Lohmann, G. P., 1986. Late Quaternary carbonate sedimentation at the Sierra Leone Rise (eastern equatorial Atlantic). *Mar. Geol.*, 70:223–250.

Gordon, A. L., 1971. Oceanography of Antarctic waters. *In* Reid, J. L. (Ed.), *Antarctic Oceanology I*: Am. Geophys. Union, Antarct. Res. Ser., 15:169–203.

Hamilton, E. L., 1971. Elastic properties of marine sediments. *J. Geophys. Res.*, 76:579–604.

Hamilton, E. L., Bachman, R. T., Berger, W. H., Johnson, T. C., and Mayer, L. A., 1982. Acoustic and related properties of calcareous deep-sea sediments. *J. Sediment. Petrol.*, 52:733–753.

Hurd, D. S., and Theyer, F., 1977. Changes in the physical and chemical properties of biogenic silica from the central equatorial Pacific: part II. Refraction index, density, and water content of acid cleaned samples. *Am. J. Sci.*, 227:1168–1202.

Kominz, M., Heath, G. R., and Moore, T. C., 1977. Bulk density of pelagic sediments from the equatorial Pacific: estimates from carbonate content, age, and subbottom depth. *J. Sediment. Petrol.*, 47:1539–1597.

Mayer, L. A., 1979. Deep-sea carbonates: acoustic, physical, and stratigraphic properties. *J. Sediment. Petrol.*, 49:819–836.

_____, 1982. Physical properties of sediment recovered on Deep Sea Drilling Project Leg 68 with the hydraulic piston corer. *In* Prell, W. L., Gardner, J. V., et al., *Init. Repts. DSDP*, 16: Washington (U.S. Govt. Printing Office), 365–382.

Micromeritics, 1978. *Instruction Manual: Sedi Graph Particle Size Analyser.*

Mienert, J., 1986. Acoustic stratigraphy in the eastern equatorial Atlantic: on the development of deep-water circulation during the last 3.5 million years. *"Meteor" Forschungsergeb., Reihe C*, 40:19–86.

Mienert, J., Curry, W. B., and Sarnthein, M., 1988. Sonostratigraphic records from equatorial Atlantic deep-sea carbonates: paleoceanographic and climatic relationships. *Mar. Geol.*, 83:9–20.

Mienert, J., and Schultheiss, P., 1989. Physical properties of sedimentary environments in oceanic high (Site 658) and low (Site 659) productivity zones. *In* Ruddiman, W. F., and Sarnthein, M., et al., *Proc. ODP, Sci. Results*, 108: College Station, TX (Ocean Drilling Program), 397–406.

Pickard, G. L., and Emery, W. J., 1982. *Descriptive Physical Oceanography. An Introduction* (4th ed.): New York (Pergamon Press).

Stein, R., 1985. Rapid grain size analyses of clay and silt fraction by Sedigraph 5000D: comparison with Coulter Counter and Atterberg methods. *J. Sediment. Petrol.*, 55:590–615.

Date of initial receipt: 28 June 1989
Date of acceptance: 8 December 1989
Ms 114B-158

Table 2. Sediment subfractions <63 μm, Site 704.

Core, section, top of interval (cm)	Depth (mbsf)	Grain-size (μm) distribution (%)															
		63–50	50–40	40–32	32–25	25–20	20–16	16–12.6	12.6–10	10–8.0	8.0–6.3	6.3–5.0	5.0–4.0	4.0–3.2	3.2–2.5	2.5–2.0	<2
114-704A-																	
1H-1, 101	1.01	0	3.0	4.0	10.0	11.0	8.5	6.5	6.0	4.0	4.0	5.0	4.0	6.0	6.0	5.0	17
1H-2, 101	2.51	0	2.0	2.5	6.0	5.0	6.0	2.5	2.5	0.5	0	2.5	5.0	10.0	6.0	6.5	43
1H-3, 101	4.01	0	1.0	4.5	5.5	6.5	5.5	5.5	4.5	3.0	3.5	3.5	5.0	5.0	6.0	5.0	36
1H-5, 112	0	0	3.0	3.0	3.0	4.0	3.5	2.5	2.5	4.5	4.0	5.0	8.0	8.0	8.0	41	
2H-1, 31	9.31	0	0.5	0.5	0	1.5	1.5	1.0	2.0	2.0	3.0	4.0	6.0	4.5	8.5	11.0	54
2H-1, 101	10.01	1.0	2.0	1.5	4.0	6.5	7.0	5.0	5.0	1.0	2.0	1.0	2.0	3.0	3.0	6.0	50
2H-2, 101	11.51	0	1.0	2.0	6.0	6.0	7.0	7.0	4.0	5.0	6.0	5.0	7.0	6.5	6.5	6.0	25
2H-3, 101	13.01	0	0	0	0.7	2.1	2.9	2.9	4.3	2.9	5.7	4.3	10.0	8.6	12.9	8.6	34
2H-4, 101	14.51	0	0	3.0	5.5	9.0	9.5	11.0	5.5	4.5	6.0	5.0	4.0	5.0	4.0	5.0	23
2H-5, 101	16.01	0.5	1.5	3.0	8.0	8.5	6.5	8.0	6.0	6.0	6.0	6.0	4.0	6.0	6.0	4.0	20
2H-6, 131	17.81	0	0	1.1	2.2	1.1	4.4	4.4	5.6	3.3	5.6	6.7	7.8	8.9	12.2	8.9	28
3H-1, 31	18.31	1.0	1.5	1.5	4.0	6.0	7.0	8.0	8.0	4.5	7.5	7.0	5.0	6.0	6.0	7.0	20
3H-1, 101	19.01	0	0	2.0	4.0	4.0	7.0	8.0	9.0	2.0	7.0	7.0	8.0	8.0	7.0	5.0	22
3H-2, 101	20.51	0	1.0	2.0	3.0	5.0	8.0	6.0	3.5	3.5	5.0	5.0	8.0	8.0	7.0	6.0	29
3H-3, 111	22.11	0	1.7	3.3	6.7	8.3	13.3	6.7	3.3	3.3	3.3	5.0	6.7	5.0	5.0	8.3	20
4H-3, 21	30.21	0	0	5.0	9.0	10.0	8.0	9.0	4.0	3.5	4.5	4.0	5.0	4.0	4.0	4.0	26
4H-3, 101	31.01	0	3.3	5.0	10.0	8.3	6.7	6.7	3.3	5.0	3.3	5.0	5.0	10.0	8.3	5.0	15
4H-5, 81	33.81	1.0	1.0	5.0	7.0	8.0	5.5	6.5	2.0	2.0	1.5	3.5	1.0	3.0	5.0	8.0	40
4H-6, 36	34.86	0.7	1.4	0	4.3	4.3	7.1	4.3	5.7	2.9	7.1	7.1	7.1	7.1	7.1	7.1	26.7
5H-1, 101	37.01	0	0	1.0	2.0	3.0	2.0	1.5	0.5	1.0	0	1.0	2.0	6.0	13.0	21.0	46
5H-3, 101	40.01	1.0	2.0	2.0	4.0	5.0	5.0	6.0	5.0	5.0	4.0	7.0	7.0	8.0	5.0	5.0	29
5H-4, 101	41.51	0	0	1.5	2.5	6.0	4.0	6.0	5.0	5.0	7.0	5.0	8.5	8.0	7.0	6.5	28
5H-5, 101	43.01	0	1.0	2.0	4.0	7.0	8.5	6.5	6.0	4.0	7.0	9.0	7.0	6.0	6.0	6.0	20
5H-6, 101	44.51	0	0	1.0	1.5	3.5	3.5	3.5	3.5	5.5	4.5	8.5	7.5	9.5	8.0	9.0	31
6H-1, 101	46.01	1.25	0	1.25	2.5	5.0	3.75	5.0	3.75	3.75	5.0	8.75	6.25	8.15	6.25	7.5	31.25
6H-3, 101	49.01	0	0	1.4	2.9	4.3	7.1	7.1	8.6	4.3	8.6	7.1	7.1	7.1	7.1	5.7	21.5
6H-4, 101	50.51	0	0	1.0	4.0	2.0	5.5	7.5	8.0	6.5	9.0	8.0	5.5	8.0	8.0	5.0	22
6H-5, 51	51.51	0	0	0.5	3.5	4.0	8.0	7.0	7.0	4.0	5.0	6.0	7.0	7.0	7.0	7.0	27
6H-5, 101	52.01	0	1.4	0.7	2.9	0.7	2.1	7.1	5.0	4.3	6.4	7.9	10.0	5.7	8.6	5.7	31.5
6H-6, 101	53.51	0	0.5	1.5	4.0	5.0	6.0	7.0	6.0	5.5	7.5	6.0	8.0	7.0	7.0	5.0	24
7H-1, 109	55.09	1.4	0	0.7	1.4	1.4	5.7	10.7	12.9	6.4	11.4	10.0	9.3	5.7	7.1	4.3	11.5
7H-2, 103	56.53	1.0	1.0	0	1.0	4.0	7.0	9.0	6.0	5.5	8.5	6.0	9.0	5.5	5.5	6.0	25
7H-3, 103	58.03	0	0	0	1.25	5.0	7.5	8.75	10.0	7.5	8.75	7.5	7.5	8.75	6.25	5.0	16.25
7H-4, 103	59.53	0	0.6	0	4.4	4.4	7.8	8.3	5.0	4.4	6.11	5.0	6.7	6.7	6.7	6.7	27.2
7H-5, 103	61.03	1.0	1.0	1.0	1.5	2.5	7.0	9.0	8.0	5.0	8.0	9.0	8.0	11.0	8.0	4.0	16
7H-6, 41	61.91	0	0	1.0	2.0	3.0	5.5	10.5	8.0	5.0	8.0	7.0	6.0	6.0	6.0	4.0	28
8H-1, 101	64.01	0	1.25	2.25	3.75	5.0	3.75	5.0	3.75	1.25	0	3.75	3.75	5.0	6.25	7.5	47.5
8H-3, 53	66.53	0.6	0.6	0	5.0	4.3	7.5	6.25	3.75	3.75	2.5	3.75	5.0	6.25	5.0	8.75	37
8H-3, 101	67.01	0	1.0	1.0	1.0	4.0	5.0	10.0	9.0	13.0	14.0	8.0	5.0	5.0	6.0	5.0	13
8H-4, 91	68.41	0	0	1.0	2.0	4.5	3.5	8.0	6.0	4.0	8.0	8.0	10.0	8.0	7.0	6.0	24
8H-5, 41	69.41	0.5	1.0	1.5	2.0	3.0	6.0	6.0	5.0	5.0	6.0	5.0	8.0	9.0	8.0	6.0	28
8H-6, 61	71.11	0	0	0	3.0	3.0	4.0	4.0	3.0	4.0	6.0	9.0	12.0	13.0	10.0	8.0	21
9H-1, 101	73.01	0.5	0.5	0	1.5	2.0	2.5	2.5	2.5	2.0	5.0	8.0	15.0	16.0	11.0	5.0	26.5
9H-2, 101	74.51	1.0	1.0	0	1.0	1.5	4.0	6.5	5.0	4.0	6.0	9.0	14.0	14.0	10.0	5.0	18
9H-3, 101	76.01	0	1.0	1.0	3.0	2.0	3.0	4.0	3.5	2.5	5.0	8.0	15.0	15.0	10.0	5.0	22
9H-4, 101	77.51	0	0	0	0	1.0	2.0	1.5	2.0	3.0	5.5	12.0	21.0	21.0	8.0	5.0	18
9H-5, 101	79.01	0	0	1.25	0	6.25	2.5	10.0	6.25	9.5	8.75	9.5	7.5	7.5	6.25	4.75	20
9H-6, 101	80.51	0	0	0	2.0	2.0	5.0	7.0	7.0	4.0	8.0	6.0	8.0	8.0	8.0	6.0	29
10H-1, 100	82.00	0	0	0	0	3.0	5.0	6.75	10.0	6.25	7.5	8.75	10.0	10.0	7.5	6.25	19
10H-2, 100	83.50	0	1.5	1.5	6.5	6.0	9.0	8.0	6.5	5.0	8.0	6.5	7.0	6.0	5.0	5.0	18.5
10H-3, 100	85.00	0.5	0.5	2.5	4.0	3.5	3.5	6.0	6.0	5.0	7.0	8.0	8.0	9.0	6.0	6.0	24.5
10H-4, 106	86.56	0	1.0	1.0	3.0	3.0	4.0	6.0	5.0	5.0	6.0	8.0	8.0	7.0	7.0	6.0	30
10H-5, 101	88.01	0	0.5	0.5	1.0	2.0	3.0	8.0	7.0	7.0	9.0	7.0	10.0	9.0	8.0	6.0	22
10H-6, 100	89.50	0	0	1.25	2.5	2.5	5.0	6.25	8.75	6.25	7.5	7.5	11.25	6.5	7.5	6.25	21

Table 2 (continued).

Core, section, top of interval (cm)	Depth (mbsf)	Grain-size (μm) distribution (%)															
		63–50	50–40	40–32	32–25	25–20	20–16	16–12.6	12.6–10	10–8.0	8.0–6.3	6.3–5.0	5.0–4.0	4.0–3.2	3.2–2.5	2.5–2.0	<2
11H-1, 100	91.00	0	0.5	1.5	2.0	4.0	3.0	4.0	4.0	4.0	6.0	8.0	10.0	10.0	9.0	7.0	27
11H-3, 101	94.01	0	0	2.0	1.0	3.0	4.0	6.0	5.0	5.5	4.5	8.0	8.0	9.0	8.0	7.0	29
11H-4, 101	95.51	0	0.5	1.0	1.0	3.5	3.0	5.0	4.5	3.5	5.0	8.0	9.0	10.0	9.0	7.0	30
11H-6, 31	97.81	0	0	0	3.0	6.0	6.0	7.0	6.0	6.0	8.0	7.0	10.0	10.0	8.0	5.0	18
11H-7, 21	99.21	0	3.0	4.0	7.5	11.0	12.0	8.0	7.0	4.0	4.0	5.0	6.0	6.0	4.0	5.0	13.5
12H-1, 59	99.51	0	1.0	1.0	1.0	3.0	3.0	5.0	3.0	4.0	6.0	11.0	14.0	11.0	8.0	5.0	24
12H-2, 59	101.09	0	0	2.0	3.0	5.0	6.0	8.0	7.0	6.0	8.0	6.0	7.0	7.0	6.5	5.0	24
12H-3, 59	102.59	0	1.0	2.0	3.0	3.0	2.5	4.5	3.0	3.5	5.0	9.0	9.5	10.0	7.0	10.0	27
12H-5, 59	105.59	0.5	0	1.5	2.0	4.0	3.0	4.0	3.5	2.0	3.5	9.0	16.0	15.0	8.0	5.0	23
12H-6, 59	107.09	0	0	2.0	3.0	3.0	4.0	4.5	4.0	3.5	10.0	14.0	17.0	10.0	6.0	4.0	15
13H-1, 101	109.01	0	0	2.0	1.0	4.0	5.5	8.0	7.5	8.0	10.0	7.0	6.0	7.0	6.0	4.0	24
13H-2, 31	109.81	1.0	1.0	2.0	3.0	3.0	3.0	6.0	3.0	4.0	6.0	8.0	12.0	10.0	8.0	6.0	24
13H-2, 101	110.51	0	1.0	0	3.0	3.0	5.0	10.0	9.0	8.0	10.0	6.0	7.0	5.0	6.0	4.0	23
13H-3, 101	112.01	0	1.0	1.0	3.5	2.0	2.5	3.0	3.0	2.5	7.5	10.0	16.0	11.0	7.0	6.0	24
13H-4, 101	113.51	0	1.0	1.5	3.5	2.5	4.0	4.0	5.0	4.0	5.0	6.0	9.0	12.0	9.0	8.0	25.5
14H-1, 101	118.01	0	0	1.5	2.5	1.5	2.0	3.5	1.0	2.0	2.5	6.5	11.0	18.0	13.0	8.0	27
14H-2, 31	118.81	0	1.0	1.0	3.0	2.5	3.0	3.5	5.0	4.0	7.5	5.0	8.0	5.0	5.0	5.0	41.5
14H-2, 101	119.51	0	1.0	2.0	2.5	3.5	4.0	4.0	2.0	3.5	4.5	8.0	12.0	13.0	10.0	6.0	24
14H-4, 101	122.51	0	1.5	0	0.5	2.0	4.0	7.0	5.0	4.0	7.0	7.0	9.0	7.0	9.0	7.0	30
14H-5, 101	124.01	0	0	2.0	2.0	5.0	3.0	4.0	6.0	4.0	8.0	12.0	12.0	8.0	7.0	5.0	22
14H-5, 131	124.31	2.0	3.5	7.0	10.5	11.0	9.0	9.0	4.0	3.0	5.0	3.0	5.0	5.5	3.5	4.0	15
15H-1, 101	127.01	0	0.5	1.5	0.5	1.5	3.0	3.0	1.0	1.0	6.0	10.0	16.0	15.0	9.0	7.0	25
15H-2, 101	128.51	0	0	0.5	3.0	3.0	6.0	4.0	3.5	3.5	7.0	10.0	12.0	10.0	8.0	6.0	23.5
15H-3, 101	130.01	0	0	0.5	1.0	3.5	5.0	6.0	5.0	3.0	7.0	11.0	13.0	9.0	7.0	6.0	22.5
15H-5, 101	133.01	0	0.5	0.5	3.0	2.0	6.0	6.0	6.0	3.5	6.0	5.5	8.0	7.0	8.0	6.0	32
16H-2, 101	137.51	0	0	0	2.9	1.4	4.3	5.7	7.1	4.3	5.7	8.6	10.0	10.0	7.1	71	25.8
16H-3, 101	139.01	0	0.5	0.5	1.5	2.0	2.0	3.0	3.0	2.5	5.0	10.5	18.0	10.0	6.0	8.0	27.5
16H-4, 101	140.51	0	0	1.5	3.0	3.0	3.0	3.0	3.0	1.5	7.0	14.0	17.0	8.0	7.0	6.0	23
16H-5, 101	142.01	0.5	1.0	0.5	2.0	4.5	4.0	5.0	4.0	4.0	5.5	5.0	7.0	7.0	8.0	7.0	35
17X-2, 101	146.51	0	2.0	1.5	1.5	3.0	2.0	2.5	3.5	1.5	7.5	13.0	17.0	9.0	8.0	4.0	24
17X-3, 101	148.01	0	1.5	4.0	4.0	7.0	8.0	6.0	6.0	4.0	6.0	6.0	5.5	5.5	9.0	5.0	22.5
17X-4, 101	149.51	0	1.0	1.0	3.0	4.0	3.0	4.0	3.0	1.5	6.5	13.0	17.0	12.0	6.0	5.0	20
17X-5, 101	151.01	0	0.5	2.5	5.0	6.5	7.5	7.5	4.5	3.0	6.0	5.0	6.0	6.0	5.0	5.0	30
18X-1, 101	154.01	0	2.0	3.0	4.0	6.0	4.0	5.0	3.5	2.0	5.5	10.5	10.5	8.0	8.0	5.0	23
18X-2, 101	155.51	0	0	2.0	3.5	3.5	4.5	5.5	4.0	3.5	5.0	4.5	6.0	7.0	8.0	8.0	35
18X-3, 126	157.26	0.5	0.5	2.0	4.0	3.5	4.5	7.0	4.0	4.0	7.0	7.0	5.5	7.5	7.0	7.0	29
18X-4, 101	158.51	1.0	1.0	0.5	3.5	2.5	4.0	4.5	1.5	2.0	7.0	12.0	18.0	10.0	8.0	5.0	20
18X-5, 101	160.01	0	0	2.0	2.0	4.0	5.0	5.0	4.0	3.5	6.0	5.5	6.0	9.0	8.0	6.0	34
18X-6, 61	161.11	0	1.1	3.3	2.2	4.4	3.3	6.7	5.6	3.3	3.9	5.6	7.8	10.0	7.8	7.8	27.2
19X-2, 101	164.51	0	0	0	2.0	2.5	0.5	3.0	2.0	1.5	1.0	3.5	5.5	7.0	8.5	15.0	48
19X-3, 101	166.01	0.5	1.0	3.0	4.0	7.0	5.0	5.0	4.0	2.0	5.0	6.0	6.0	2.2	7.0	7.0	35.5
19X-4, 101	167.51	0	0	1.0	3.0	1.0	2.0	3.0	0.5	0.5	1.5	2.0	2.5	5.0	17.0	27.0	34
19X-5, 101	169.01	0	0	1.0	1.0	0	1.0	2.5	1.5	1.5	3.0	4.0	6.5	10.0	8.0	7.0	53
19X-6, 101	170.51	0	0	0.5	2.5	3.0	2.0	3.5	1.0	0	1.0	3.0	4.0	2.5	8.0	17.0	52
20X-1, 101	172.01	0	1.0	0.5	1.5	1.0	3.0	3.5	1.0	1.5	5.0	8.0	10.0	6.0	6.0	5.0	47
20X-2, 101	173.51	0	1.0	2.0	2.0	2.0	4.0	3.0	2.0	1.5	5.0	7.0	9.0	8.5	7.5	8.0	38
20X-3, 101	175.01	0	0	1.0	1.5	1.5	2.0	2.5	1.0	2.5	4.0	11.0	11.0	7.0	5.0	6.0	44
20X-4, 101	176.51	0	0	0.5	1.0	1.5	1.5	1.0	1.5	3.0	5.5	13.0	10.5	4.0	5.0	9.0	43
20X-5, 101	178.01	0	0	1.0	1.0	4.0	4.0	4.5	3.5	3.0	6.0	14.0	9.0	6.0	5.0	6.0	33
20X-6, 101	179.51	0	0	2.0	3.0	3.5	2.0	2.5	4.0	2.0	9.0	17.0	11.0	5.0	6.0	6.0	27
21X-1, 101	181.01	1.0	0.5	1.5	4.0	2.0	2.0	3.0	2.5	3.5	12.0	16.0	6.0	5.0	7.0	10.0	24
21X-2, 101	182.51	0	0	3.5	3.0	2.5	2.0	3.0	0.5	3.0	11.5	19.5	8.5	4.5	4.5	5.5	31
21X-3, 101	184.01	0	1.0	2.0	6.0	3.0	4.0	1.0	2.0	2.0	10.0	14.0	6.0	3.0	2.5	3.5	40
21X-4, 71	185.21	0	1.0	0	2.0	2.0	3.0	3.5	0.5	4.0	7.5	9.0	7.5	12.0	9.0	7.0	32
22X-1, 101	190.01	0	2.0	1.5	5.5	5.0	3.0	5.5	2.5	3.0	4.0	8.0	10.0	7.0	6.0	5.0	32

Table 2 (continued).

Core, section, top of interval (cm)	Depth (mbsf)	Grain-size (μm) distribution (%)															
		63–50	50–40	40–32	32–25	25–20	20–16	16–12.6	12.6–10	10–8.0	8.0–6.3	6.3–5.0	5.0–4.0	4.0–3.2	3.2–2.5	2.5–2.0	<2
22X-2, 101	191.51	0	0.5	0.5	1.0	2.0	2.0	2.5	1.5	1.5	4.5	8.0	12.0	11.0	8.0	7.0	38
22X-3, 101	193.01	0	0	0	1.5	0	2.0	1.0	1.5	1.0	5.5	10.0	7.5	11.0	8.5	8.0	42.5
22X-4, 101	194.51	0	0	0.5	1.0	0	1.0	0	0	1.0	3.0	6.0	15.0	11.0	9.0	9.0	43.5
22X-5, 101	196.01	0.5	0	0.5	2.5	0	0.5	0	0.5	0	2.5	2.0	10.5	19.0	15.0	13.0	33.5
23X-1, 101	199.01	1.0	0	3.0	4.0	4.0	5.0	2.0	3.5	1.5	6.0	11.0	13.0	8.0	8.0	7.0	23
23X-2, 101	200.51	0.5	0.5	2.0	3.0	3.5	3.5	3.0	4.0	1.0	4.0	8.0	11.0	8.0	7.0	7.0	34
23X-3, 101	202.01	1.5	1.0	4.0	3.0	5.5	5.5	5.0	3.5	1.5	6.5	13.5	11.0	7.0	4.0	5.0	22.5
23X-4, 101	203.51	0	0	1.0	1.5	5.0	3.5	3.5	5.0	3.0	3.0	6.0	8.5	9.0	8.0	8.0	35
23X-5, 101	205.01	0.5	1.0	0.5	2.0	2.5	2.5	3.0	3.0	1.0	6.0	6.0	12.0	9.0	10.0	10.0	31
24X-2, 83	209.33	1.0	0	0.5	2.0	2.5	4.0	2.0	3.0	2.0	4.0	7.0	8.0	9.0	9.0	8.0	38
24X-3, 83	210.83	0.5	0.5	0.5	1.0	1.0	2.0	0.5	0.5	0.5	2.0	5.0	9.0	11.0	10.0	10.0	46
24X-4, 83	212.83	0.5	0.5	1.0	2.0	1.0	1.0	3.0	2.5	1.5	3.0	4.5	6.5	10.0	8.0	7.0	48
24X-5, 83	212.83	0.5	1.0	1.0	0.5	2.0	2.5	1.5	1.5	1.5	3.0	5.0	11.0	13.0	10.0	7.0	39
25X-1, 131	217.31	0	0.5	0.5	0.5	0.5	1.0	1.0	1.0	1.0	3.0	4.0	6.0	9.0	9.0	8.0	55
25X-2, 131	218.81	0	0	0	1.0	0	0.5	0.5	1.0	1.5	2.5	5.0	6.0	7.0	8.0	8.0	59
25X-3, 91	219.91	1.0	0	0	1.0	1.0	1.0	1.0	1.0	0.5	5.0	10.5	12.0	9.0	9.0	8.0	40
25X-4, 91	221.41	0	0	1.0	1.0	0.5	0.5	1.0	2.0	1.0	2.0	6.0	8.0	9.0	9.0	8.0	51
25X-5, 51	222.51	0	0	0.5	2.5	0	1.5	1.0	0	1.0	2.5	9.0	12.0	12.0	10.0	7.0	41
25X-6, 51	224.01	0	1.25	0	1.25	0	1.25	3.75	2.5	2.5	1.25	5.0	6.25	10.0	10.0	7.5	47.5
114-704B-																	
26X-1, 101	226.01	0	0.5	0	1.5	1.0	0.5	1.5	1.0	1.0	2.0	6.0	9.0	12.0	9.0	9.0	46
26X-2, 101	227.51	0	0.5	0.5	1.0	2.0	0.5	3.5	2.0	3.0	6.0	7.0	7.0	8.0	8.0	8.0	43
26X-3, 101	229.01	0.5	0.5	0.5	0.5	1.0	2.0	2.0	0	1.0	2.0	4.0	7.0	10.0	8.0	8.0	53
26X-4, 101	230.51	0.5	0.5	0	0.5	1.5	1.5	0.5	1.0	1.0	4.5	3.5	7.0	12.0	9.0	8.0	49
27X-2, 101	236.51	0.5	0.5	0.5	0.5	0.5	1.5	1.0	0	0.5	2.0	5.5	9.0	9.0	12.0	9.0	48
27X-3, 61	237.61	0	0	0	1.0	1.0	1.0	1.5	1.5	4.0	5.0	7.0	9.0	9.0	9.0	8.0	43
27X-4, 101	239.51	0	1.0	0	0	1.0	2.5	0.5	0.5	0	3.5	8.0	11.0	13.0	11.0	11.0	37
27X-5, 76	240.76	0	2.0	1.0	2.0	1.5	3.5	1.0	3.0	1.0	2.5	6.5	6.0	9.0	7.0	9.0	50
27X-6, 101	242.51	0	0	0	1.5	0	1.5	1.0	0	2.0	4.0	9.0	10.0	7.0	8.0	7.0	49
28X-1, 111	244.11	0	0.5	0.5	1.0	2.0	1.5	0.5	1.0	0.5	6.5	13.0	13.0	9.0	8.0	6.0	37
28X-2, 111	245.61	1.0	0	1.5	3.5	5.0	4.0	3.0	2.0	2.0	7.0	11.0	8.0	7.0	8.0	4.0	33
28X-3, 111	247.11	0	0	0	1.0	2.0	1.0	1.0	0.5	0	4.5	13.0	18.0	14.0	10.0	8.0	27
28X-4, 101	248.51	0	0.5	1.5	1.0	0.5	1.0	0.5	1.0	0	3.0	10.0	14.0	16.0	11.0	11.0	29
28X-5, 101	250.01	0	0	1.0	1.0	0.5	2.5	0	0.5	1.5	7.0	14.0	17.0	10.0	9.0	8.0	28
28X-6, 101	251.51	0	0	1.0	2.0	3.0	2.0	1.0	1.0	0	3.5	8.5	15.0	13.0	10.0	8.0	32
29X-1, 91	252.91	0	1.0	4.0	5.0	4.0	4.0	6.0	1.0	2.0	5.0	12.0	12.0	9.0	5.0	5.0	25
29X-2, 91	254.41	0.5	0	1.5	0.5	1.5	2.0	0	0	2.0	7.5	16.5	16.0	10.0	8.0	8.0	26
29X-3, 91	255.91	0	0.5	1.5	3.5	3.0	1.5	3.5	0	0	4.0	9.0	12.0	9.0	9.0	6.0	37.5
29X-4, 91	257.41	1.0	1.5	0.5	1.5	1.5	3.0	1.0	1.0	1.0	3.0	11.0	12.0	11.0	10.0	9.0	32
29X-5, 91	258.91	0	1.0	1.0	1.0	1.0	3.0	0.5	1.5	2.0	6.5	8.5	11.0	9.0	8.0	9.0	37
29X-6, 91	260.41	1.0	1.0	1.0	1.0	3.0	1.0	2.0	1.0	1.0	4.0	7.0	11.0	10.0	7.0	8.0	41
30X-1, 101	262.01	0.5	0.5	1.0	2.0	2.0	3.0	2.0	1.0	2.0	6.0	12.0	10.0	9.0	7.0	5.0	37
30X-2, 101	263.51	0	1.0	3.0	7.0	7.0	4.0	5.0	3.5	2.0	3.5	5.0	7.0	8.0	5.0	9.0	30
30X-3, 101	265.01	1.0	0	1.0	1.0	1.0	1.0	0	2.0	8.0	18.0	20.0	10.0	10.0	6.0	20	
30X-4, 101	266.51	0.5	1.5	2.0	4.0	4.5	2.5	1.0	3.0	1.0	3.0	9.0	10.0	10.0	7.0	9.0	32
31X-1, 101	271.01	0	0.5	0	2.5	2.0	2.0	0.5	1.5	2.5	6.5	9.0	13.0	10.0	9.0	9.0	32
31X-2, 101	272.51	0	1.0	0	1.0	1.0	1.0	2.0	2.0	2.0	10.0	12.0	12.0	9.0	8.0	7.0	32
31X-3, 101	274.01	1.0	1.0	1.5	0	0.5	1.0	1.0	1.5	0	3.5	9.0	12.0	13.0	12.0	13.0	30
31X-4, 101	275.51	0	0	0	0	1.0	1.5	1.5	4.0	4.5	15.5	14.5	10.5	7.0	7.5	6.0	26.5
31X-5, 101	277.01	0	1.0	0	0.5	2.5	2.0	1.0	1.0	2.0	8.5	14.5	14.0	9.0	8.0	8.0	28
31X-6, 101	278.51	0	0	1.0	3.0	3.0	3.0	2.0	1.0	1.5	3.5	8.0	10.5	10.5	9.0	8.0	36
32X-1, 101	280.01	0	1.0	1.0	1.0	1.0	1.0	2.5	2.0	3.0	10.5	14.5	9.5	8.0	7.0	5.0	33
32X-2, 101	281.51	1.0	0	0	1.0	1.0	1.0	1.0	3.0	2.0	10.0	14.0	11.0	8.0	8.0	7.0	32
32X-3, 101	283.01	0	0	0.5	1.5	0.5	1.5	0	1.0	3.0	9.0	13.0	12.0	12.0	9.0	7.0	30

Table 2 (continued).

Core, section, top of interval (cm)	Depth (mbsf)	Grain-size (μm) distribution (%)															
		63–50	50–40	40–32	32–25	25–20	20–16	16–12.6	12.6–10	10–8.0	8.0–6.3	6.3–5.0	5.0–4.0	4.0–3.2	3.2–2.5	2.5–2.0	<2
32X-4, 101	284.51	0	0	1.0	1.0	1.0	0	0	2.0	1.5	8.5	12.0	15.0	12.0	10.0	9.0	27
32X-5, 101	286.01	0	0	1.0	1.0	2.0	3.0	1.0	0.5	1.5	7.0	10.0	11.0	11.0	8.0	8.0	35
32X-6, 101	287.51	0	1.0	3.0	3.0	2.0	2.0	3.0	0	0	3.0	6.0	10.0	10.0	8.0	7.0	42
33X-1, 101	289.01	0	1.0	0	0.5	1.0	0.5	3.0	2.0	6.5	15.5	13.0	9.0	7.0	8.0	6.0	27
33X-2, 101	290.51	0	0	1.5	1.5	2.0	1.0	1.5	1.5	2.0	10.0	15.0	17.0	9.0	8.0	5.0	25
33X-3, 101	292.01	0	1.0	1.5	2.5	1.0	0	0.5	3.0	1.5	10.0	13.0	14.0	11.0	7.0	9.0	25
33X-4, 101	293.51	0	0	0	1.0	2.0	1.0	0	2.5	0.5	9.0	11.0	14.0	10.0	10.0	9.0	30
33X-5, 101	295.01	0	0	0.5	1.0	0.5	1.0	0	1.0	0	1.0	8.0	13.0	12.5	10.5	10.0	41
33X-6, 101	296.51	0.5	0.5	1.0	2.0	3.0	2.0	3.0	2.0	0.5	3.5	7.0	12.0	10.0	9.0	8.0	36
34X-1, 101	298.01	1.0	0	1.0	1.0	2.0	0.5	0.5	0	0	0.5	4.5	8.0	13.0	17.0	18.0	33
34X-2, 101	299.51	0	0	1.0	0	1.0	1.0	1.0	1.0	3.5	6.0	13.5	12.0	7.0	7.0	10.0	36
34X-3, 101	301.01	0.5	1.0	0	1.5	1.5	1.0	1.0	3.0	3.0	11.0	14.0	11.0	9.0	9.0	9.0	24.5
34X-4, 101	302.51	1.0	0	0.5	0.5	0.5	0.5	3.0	2.5	5.5	15.0	12.0	11.0	7.0	8.0	8.0	25
34X-5, 101	304.01	1.0	0	1.0	1.0	0	1.0	2.5	1.5	3.0	10.5	15.5	11.0	8.0	8.0	6.0	30
34X-6, 101	305.51	0	0	1.0	0.5	1.0	0.5	2.0	0	1.0	9.0	12.5	13.5	9.0	7.0	7.0	35
35X-1, 101	307.01	0.5	0.5	2.5	0	0.5	1.0	1.5	0	1.0	6.5	12.5	11.0	10.0	8.0	8.0	36.5
35X-2, 101	308.51	0	0.5	0.5	2.5	1.5	0.5	1.5	2.5	1.5	3.5	8.0	11.0	10.0	10.0	9.0	37
35X-3, 101	310.01	0.5	1.5	1.0	2.0	1.0	3.0	3.0	0.5	3.5	3.0	6.0	9.0	9.0	10.0	6.0	41
35X-4, 101	311.51	0	0	0.5	1.5	1.0	1.0	3.5	2.0	2.5	6.0	7.0	6.0	9.0	9.0	9.5	41.5
35X-5, 101	313.01	0.5	0.5	1.0	2.5	2.5	2.0	4.0	0.5	2.5	5.5	9.5	8.0	8.0	7.0	6.0	40
35X-6, 101	314.51	1.0	1.0	1.0	3.0	4.0	2.5	3.0	1.0	1.5	2.0	6.0	8.0	6.0	8.0	6.0	46
36X-1, 101	316.01	0	0	1.0	0.5	1.0	1.5	0.5	0.5	1.0	5.0	13.5	14.5	8.0	6.0	9.0	39
36X-2, 98	317.48	0.5	0	0	2.0	0	1.0	1.0	0	0	4.0	11.5	14.5	11.0	9.0	9.0	35.5
37X-2, 101	326.51	1.0	0	0	1.5	0.5	1.0	0.5	2.5	0	1.0	6.0	13.0	11.0	10.0		
37X-3, 101	328.01	0	0	0	1.0	1.0	1.0	1.0	1.0	0	0	6.0	12.0	12.0	13.0	12.0	40
39X-1, 101	343.01	1.0	0	0.5	0	2.0	2.0	2.0	1.0	1.0	6.0	11.0	15.0	9.0	9.0	8.0	33
39X-2, 101	344.51	0.5	0.5	0.5	0.5	2.0	0.5	1.5	1.0	2.0	8.0	11.0	11.0	8.0	7.0	5.0	41
39X-3, 101	346.01	0	0.5	0.5	2.0	1.0	1.0	0	1.0	0	6.0	12.0	14.5	8.5	8.0	8.0	37
39X-4, 101	347.51	0.5	0.5	0.5	1.0	0.5	2.0	0.5	1.5	0	8.0	15.0	13.0	8.0	9.0	7.0	33
39X-5, 101	349.01	0	1.5	0	2.0	1.0	0	1.0	0	0	3.0	8.0	16.0	13.0	10.0	9.0	35
39X-6, 101	350.51	1	0.5	0.5	2.5	1.0	0	0	1.0	1.5	2.5	8.0	12.0	12.0	11.0	12.0	35
40X-1, 99	351.99	0.5	1.0	1.0	0	1.0	1.0	1.0	1.0	1.0	4.0	10.0	15.0	9.0	8.0	7.0	40
40X-2, 99	353.49	0	0.5	1.0	1.0	1.0	0.5	1.0	1.0	0	3.0	9.0	13.0	9.5	8.5	9.0	42
40X-3, 99	354.99	1.0	1.0	1.0	0	1.0	0.5	1.0	0.5	0	4.0	9.0	11.0	8.0	10.0	11.0	41
40X-4, 99	356.49	0.5	0.5	0.5	2.0	1.0	1.0	1.0	0	0	3.0	8.0	12.0	7.0	8.0	9.0	46
40X-5, 99	357.99	0	0	0.5	0.5	2.0	1.0	0	0.5	0.5	3.0	11.0	10.0	8.0	8.0	9.0	46
40X-6, 99	359.49	0	1.0	0.5	0.5	3.0	1.5	0	0	1.5	4.5	8.5	12.0	9.0	8.0	7.0	43
41X-1, 102	361.02	0	0.5	1.0	1.0	1.5	0.5	0	0	0.5	4.5	9.0	16.0	11.0	9.0	7.0	39
41X-2, 102	362.52	0	0	0	0.5	0.5	1.5	0.5	0	1.5	1.5	6.0	15.0	13.5	9.5	6.5	42.5
41X-3, 102	364.02	1.0	0	0	1.0	1.0	2.0	1.0	0.5	1.5	2.0	10.0	17.0	11.0	10.0	6.0	36
41X-4, 101	365.52	0	1.0	0	2.0	1.5	0	0	0	0	4.5	11.0	12.0	11.0	12.0	5.0	40
41X-5, 102	367.02	1.5	0	1.5	1.0	1.0	0	1.0	0	0	1.0	9.0	16.0	13.0	1.0	9.0	37.5
41X-6, 102	368.52	0	0.5	0	1.0	1.0	0	1.0	0	0	3.0	8.0	14.0	10.0	10.0	8.0	42
42X-2, 100	371.50	0	0	1.0	2.0	0	2.5	1.5	1.0	1.5	6.5	13.0	10.0	8.0	10.0	7.0	37
42X-4, 100	374.50	0	0	0	0	2.0	0.5	0.5	1.0	0	3.0	9.0	15.0	9.0	8.0	6.0	45
42X-6, 100	377.50	0	0	0.5	2.0	2.0	1.0	1.0	0	1.0	6.0	11.0	11.0	8.0	9.0	8.0	40
43X-1, 101	379.01	0	0.5	0	1.0	1.0	0	1.0	0	1.0	6.0	12.0	12.5	9.5	8.0	7.0	40
43X-4, 101	383.51	0	1.0	1.0	1.0	1.0	1.0	0.5	0.5	0	4.0	7.5	8.5	8.0	7.0	8.0	52
43X-7, 51	387.51	0	0.5	0.5	1.0	2.0	0	0	0	0	4.0	10.0	12.0	8.0	9.0	10.0	42.5
44X-1, 101	388.01	0.5	0.5	0.5	2.0	1.5	0	1.0	1.0	0	2.5	7.5	11.0	14.0	10.0	8.0	40
45X-1, 102	397.02	0	1.0	1.5	1.0	0.5	1.5	0.5	0	0.5	2.5	8.0	14.0	13.0	10.0	10.0	37
45X-2, 102	398.52	0	0.5	0.5	0	1.0	1.0	0	0	1.0	4.0	11.0	14.0	10.0	7.0	8.0	41
46X-2, 102	407.52	1.0	0.5	2.0	1.0	1.0	0	0	3.5	0	5.0	19.5	22.0	12.0	9.5	6.5	21.5
46X-3, 102	409.02	0.5	0.5	4.5	2.0	4.0	1.0	2.0	2.0	2.0	6.5	9.0	18.0	10.0	9.0	6.0	24
46X-4, 95	410.45	1.0	3.0	1.0	6.5	4.0	5.0	3.5	2.0	1.0	0.5	6.0	11.0	12.0	9.0	7.5	23.5

Table 2 (continued).

Core, section, top of interval (cm)	Depth (mbsf)	Grain-size (μm) distribution (%)														
		63–50	50–40	40–32	32–25	25–20	20–16	16–12.6	12.6–10	10–8.0	8.0–6.3	6.3–5.0	5.0–4.0	4.0–3.2	3.2–2.5	2.5–2.0	<2
47X-2, 91	416.41	0	1.0	1.0	2.5	2.5	3.0	2.0	2.0	1.0	6.0	8.0	10.0	10.0	9.0	7.0	35
47X-3, 91	417.91	1.0	2.0	1.5	2.0	3.5	1.5	0	3.0	1.0	2.0	10.0	12.0	8.5	8.5	7.0	38
47X-4, 91	419.41	0	0.5	1.5	1.0	1.0	2.0	3.0	1.5	0	4.0	11.0	15.0	10.0	8.0	7.0	33
47X-5, 91	420.91	0.5	1.0	1.0	2.0	2.5	3.0	2.5	0.5	1.0	5.5	9.0	11.0	7.0	8.0	8.0	36
47X-6, 91	422.41	0	0.5	1.0	1.5	1.0	2.0	1.0	1.0	1.5	1.5	8.5	16.0	15.0	8.0	8.0	34
48X-1, 101	424.01	0	0	1.5	1.0	2.0	2.0	1.0	0	0.5	2.5	8.0	18.0	15.0	8.0	8.0	32
48X-2, 101	425.51	1.0	0.5	1.5	1.0	0	0.5	0	2.0	0	2.0	8.0	11.5	14.0	14.0	10.0	36
48X-3, 101	427.01	0.5	1.5	1.5	1.0	3.5	2.5	1.5	2.0	1.0	3.0	8.0	16.0	16.0	10.0	6.0	26.5
49X-1, 101	433.01	1.0	2.0	3.0	6.5	3.0	5.0	4.0	3.0	2.0	1.5	5.5	11.5	15.0	9.0	7.0	24
49X-2, 84	434.34	1.0	1.5	2.5	5.0	6.0	3.0	5.0	0.5	1.5	4.5	9.0	10.0	9.0	7.0	6.0	25.5
49X-3, 85	435.85	0	0.5	3.0	2.0	3.0	4.0	3.0	1.0	1.5	4.0	10.0	20.0	13.0	9.0	6.0	21
49X-4, 85	437.35	0	0	5.0	4.5	5.0	4.0	2.5	4.5	2.0	4.0	11.0	16.0	11.0	7.0	6.0	23
49X-5, 50	438.50	0	3.0	3.5	8.0	7.0	6.0	6.5	3.0	4.0	5.0	6.0	9.0	6.0	7.0	6.0	17
49X-5, 136	439.36	1.0	0	1.0	5.5	3.0	4.0	2.0	0	1.5	3.0	6.5	15.0	14.0	9.0	7.0	22
50X-1, 54	441.54	1.0	1.0	0	0	1.0	0.5	0.5	1.0	0	0	4.0	13.0	21.0	13.0	11.0	33
51X-1, 50	450.50	0.5	0.5	0	0	3.0	1.0	1.0	0	0	2.0	7.0	15.0	15.0	11.0	10.0	33
52X-1, 48	459.48	0	0	1.0	2.0	2.0	2.0	1.0	0.5	0	4.0	8.0	15.0	14.0	9.0	9.0	34
52X-2, 48	460.98	0	0	0	2.0	1.0	1.0	1.5	1.0	1.0	2.5	12.5	13.0	11.0	9.0	8.0	36

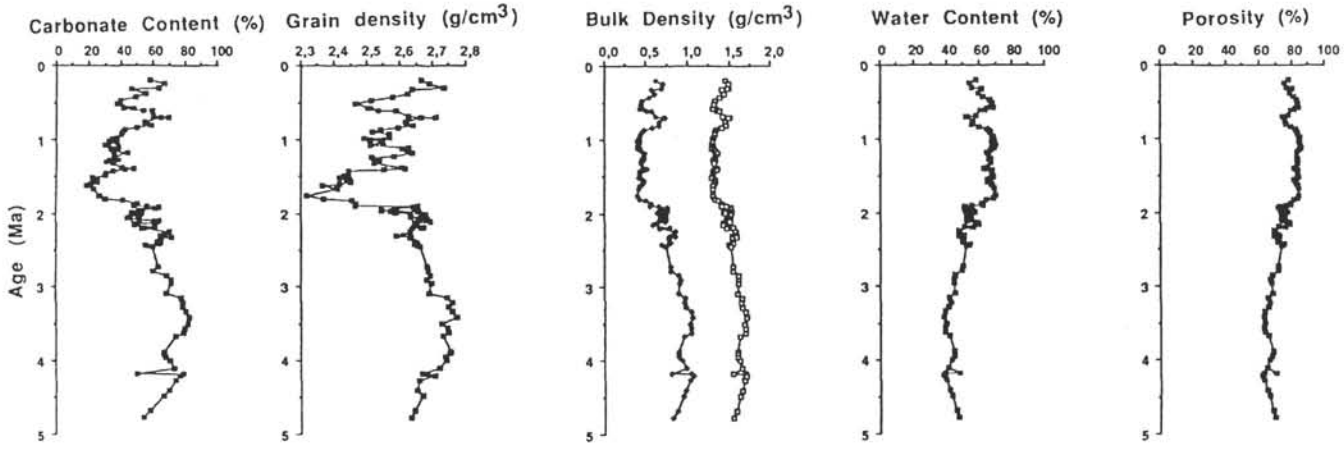

Figure 7. Correlation of carbonate content, grain density, bulk density, water content, and porosity vs. age.

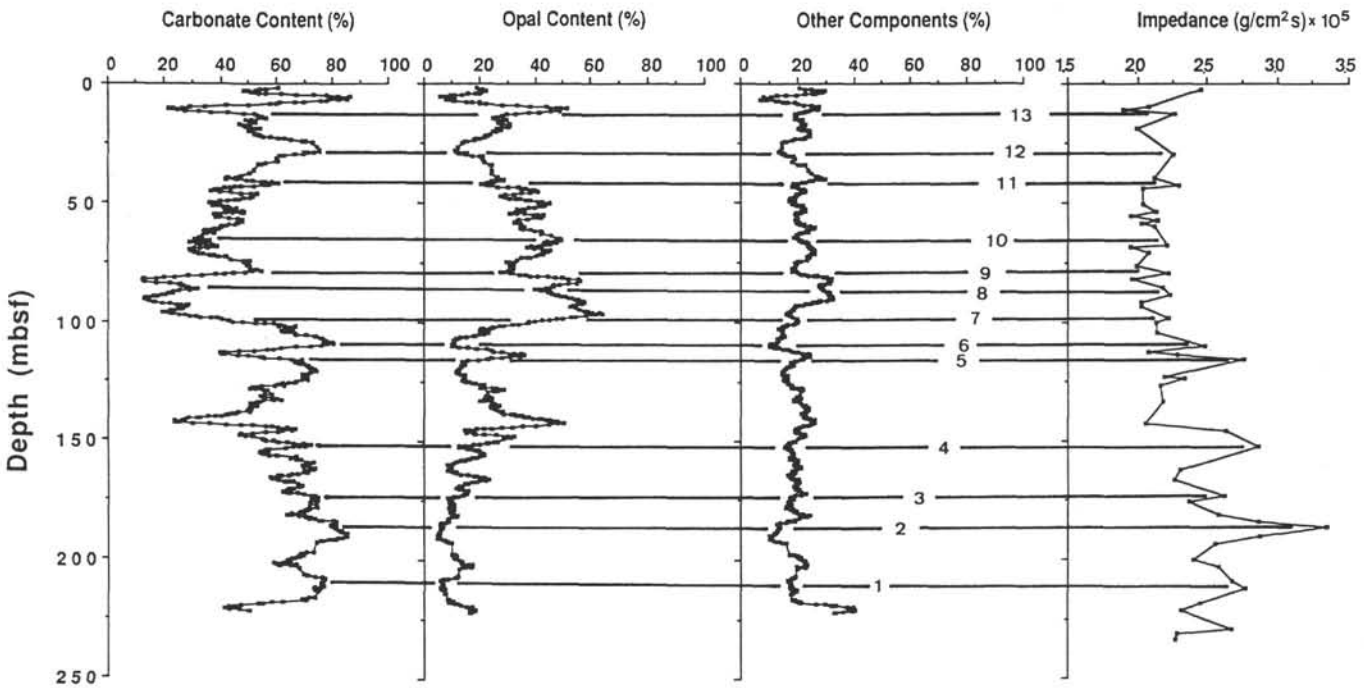

Figure 8. Correlation between carbonate content, biogenic opal content, other components, and impedance vs. depth. The high-resolution biogenic opal, other components, and carbonate content data (from Froelich et al., this volume) are smoothed by taking the average value of 10 measurements.

Table 3. Summary of impedance peaks associated with changes in the concentration of biogenic silica and carbonate content.

Impedance peak	$\Delta CaCO_3$ (%)	ΔSiO_2 (%)	ΔOther components (%)	Age[a] (Ma)	Depth (mbsf)
1	20	10	15	4.6	211
2	25	5	10	3.5	187
3	14	10	5	2.8	173
4	15	14	5	2.4	152
5	30	35	10	2.1	116
6	43	25	15	2.0	110
7	46	40	8	1.9	98
8	12	18	15	1.7	87
9	40	30	12	1.5	78
10	10	15	12	1.3	66
11	25	22	8	1.0	42
12	35	15	10	0.8	30
13	35	20	8	0.5	13

[a] Based on biostratigraphic and paleomagnetic datum levels from Table 1.